Dalton Transactions

PAPER

View Article Online
View Journal | View Issue

Cite this: *Dalton Trans.*, 2018, **47**, 1159

The effect of functional groups in the aqueous-phase selective sensing of Fe(III) ions by thienothiophene-based zirconium metal–organic frameworks and the design of molecular logic gates†

Rana Dalapati,[a] Ülkü Kökçam-Demir,[b] Christoph Janiak [b] and Shyam Biswas *[a]

Received 2nd November 2017,
Accepted 8th December 2017

DOI: 10.1039/c7dt04130f

rsc.li/dalton

The synthesis of four isoreticular, water-stable Zr(IV) metal–organic frameworks (MOFs) was conducted under solvothermal conditions by using thienothiophene-based ligands. The MOFs were fully characterized by XRPD analyses, FT-IR spectroscopy and TG analyses. The ligands were systematically modified with methyl and phenyl groups for tuning the fluorescence and hydrophobic behaviour of the MOFs. The photophysical properties of free ligands and the corresponding MOFs were investigated by steady-state as well as time-resolved fluorescence experiments. The MOFs containing π-electron rich, conjugated thieno[3,2-*b*]thiophene units were employed for the sensing of metal ions. All the MOFs displayed high selectivity and sensitivity towards the sensing of biologically important Fe^{3+} ions in pure aqueous medium through the fluorescence quenching mechanism. Detailed experimental investigations suggest that the transfer of electrons from the electron-rich frameworks to the half-filled 3d orbitals of Fe^{3+} ions results in fluorescence quenching. Surprisingly, the electron acceptor methyl viologen (MV^{2+}) ions exhibited a reverse trend in the quenching efficiency compared to the Fe^{3+} ions. Both the steric and electronic effects of the attached functional groups can be proposed to play determining roles in the fluorescence quenching mechanism. All the MOFs showed high photostability and reusability, which are beneficial for the long-term real-world detection of Fe^{3+} ions. Interestingly, the MOFs can be utilized to construct molecular logic gates for the efficient discrimination between Fe^{3+} and Fe^{2+} ions.

Introduction

Over the past few decades, the selective recognition of biologically active species has been one of the devoted areas of scientific research.[1] Among the various methodologies, the fluorescence-based molecular recognition strategy has gained significant attention due to its simplicity and high sensitivity. Recently, metal–organic frameworks (MOFs)[2] have been efficiently employed in many fields including chemical separation,[3] gas storage,[4] heterogeneous catalysis,[5] polymerization[6] and drug delivery.[7] Another propitious field of application for MOFs is fluorescence sensing. Fluorescent MOFs have several advantages over the conventional small-molecule-based sensor materials because of their ultrahigh surface areas, adjustable porosities, functionalizable pore walls and π-conjugated backbones.[8] The ordered orientation of fluorescent ligands and metal clusters in MOFs enhances the rate of electron transfer throughout the framework.[9,10] In addition, the porous channels inside the frameworks can act as the space for external analytes and improve the electronic communication between the receptor along the framework and the analyte.[11] Encouraged by the advantages of MOF-based fluorescent sensor materials, significant research efforts have been devoted to date to prepare MOFs for the optical/fluorescence sensing of ionic species, small organic molecules, volatile organic compounds and energetic materials.[12,13] The metal ions and organic ligands can be wisely selected to prepare MOFs (under suitable reaction conditions) possessing the desired fluorescence sensing behaviour. However, such targeted design and synthesis of MOFs having high selectivity towards the detection of a particular analyte is still a challenging task.

[a]*Department of Chemistry, Indian Institute of Technology Guwahati, 781039 Assam, India. E-mail: sbiswas@iitg.ernet.in; Fax: +91-3612582349; Tel: +91-3612583309*
[b]*Institut für Anorganische Chemie und Strukturchemie, Universität Düsseldorf, Universitätsstraße 1, 40225 Düsseldorf, Germany*

†Electronic supplementary information (ESI) available: IR spectra, TG curves, XRPD patterns, absorption and fluorescence spectra, water sorption isotherms, EDX spectra, and life-time decay profiles. See DOI: 10.1039/c7dt04130f

Among the biologically active cations, sensing of Fe^{3+} is one of the important areas of research since it is actively involved in biological processes like storage and transport of oxygen,[14] electron transfer as well as the synthesis of DNA and RNA.[15] The permissible limit of iron in drinking water is 0.3 mg mL^{-1}, which has been recommended by the World Health Organization (WHO).[16] The excess levels of iron cause cellular toxicity,[17,18] which can damage biomolecules (such as lipids and proteins)[19] and may be associated with some serious diseases such as Alzheimer's disease.[20] Thus far, several fluorescent MOFs have been developed to recognize Fe^{3+} ions.[21–23] However, there has been no report on the discrimination between Fe^{3+} and Fe^{2+} ions by MOF materials so far. For the detection of Fe^{3+} ions, numerous lanthanide-based[23–26] MOFs have been used owing to their excellent luminescence properties. A few non-lanthanide[27,28] MOFs have also been employed for serving the same purpose. However, most of the previously reported lanthanide MOF-based fluorescent sensors for Fe^{3+} ions work *via* cation-exchange with framework metal ions.[28] The cation-exchange mechanism leads to either the collapse of the framework[29] or the generation of mixed-metal frameworks.[30] As a result, these MOF-based fluorescent probes show poor recyclability of their detection performances towards Fe^{3+} ions. Moreover, other cations (*e.g.* Al^{3+}, Cu^{2+}) have been reported to interfere with the recognition of Fe^{3+} ions. Therefore, the development of MOF-based sensor materials for Fe^{3+} ions that can overcome the above-stated problems is still a challenging task. In addition to the fluorescence quenching *via* the cation-exchange mechanism, the interactions of Fe^{3+} ions with the organic ligands and simultaneous electron transfer from the electron-rich frameworks to the electron-poor Fe^{3+} ions can also lead to fluorescence quenching.[31]

Numerous Zr(IV)-based MOFs have been reported to exhibit high physicochemical stabilities.[32,33] Therefore, the synthesis of Zr(IV) MOFs containing fluorescent ligands could be a better choice than the lanthanide-based MOFs in order to resist the structural collapse of the MOFs during the sensing events. Furthermore, the use of highly conjugated ligands might facilitate the electron shuttle from the framework to the electron-poor species of interest. Owing to its highly extended π-electron system, there is an extensive use of the thieno[3,2-*b*] thiophene species for the preparation of high-performance organic polymer semiconductors.[34–36] Therefore, we hypothesized that the construction of Zr(IV) MOFs incorporating thienothiophene units could be very effective for showing fluorescence quenching behavior towards Fe^{3+} ions through the electron transfer mechanism. In this work, the preparation and thorough characterization of four highly stable Zr(IV) MOFs (three new and one previously reported[37] by us) containing thienothiophene-based ligands are presented. All the MOFs were capable of performing selective sensing of Fe^{3+} ions in pure aqueous medium by the fluorescence quenching mechanism. The fluorescence sensing behavior of the MOFs towards Fe^{3+} ions has been systematically tuned by grafting methyl and phenyl groups with thienothiophene-based ligands. The dynamic nature of the fluorescence quenching processes in these MOF systems has been indicated by the fluorescence investigations (both steady-state and time-resolved). The presence of the electron transfer mechanism was confirmed by employing the well-known electron acceptor methyl viologen (MV^{2+}) dications, which exhibited a reverse trend in the fluorescence quenching efficiencies of the MOFs compared to the Fe^{3+} ions. It has been anticipated that both the steric and electronic effects of the functional groups grafted with thienothiophene-based ligands govern the fluorescence quenching mechanism. In addition to the selective sensing of Fe^{3+} ions, molecular logic gates were constructed by using the MOFs for discrimination between Fe^{3+} and Fe^{2+} ions.

Experimental

Materials and physical measurements

The preparation of H_2TDC, H_2DMTDC, H_2MPTDC and H_2DPTDC ligands was carried out by following literature protocols.[38] All other reagents were procured from the commercial vendors. All the fluorescence titration experiments were conducted by using Milli-Q water as a medium. A PerkinElmer Spectrum Two FT-IR spectrometer (FT-IR = Fourier transform infrared) was employed to collect the FT-IR spectra in the region of 440–4000 cm^{-1}. For characterizing the absorption peaks, the following notations were used: weak (w), medium (m), strong (s), very strong (vs), shoulder (sh) and broad (br). A Mettler-Toledo TGA/SDTA 851e thermogravimetric instrument was utilized to carry out the thermogravimetric analysis (TGA) in the temperature range of 30–700 °C in air at a heating rate of 5 °C min^{-1}. X-Ray powder diffraction (XRPD) patterns were obtained at room temperature with a Bruker D2 Phaser X-ray diffractometer functioning at 30 kV and 10 mA employing Cu-Kα (λ = 1.5406 Å) radiation. UV-Vis spectra were recorded with a PerkinElmer Lambda 25 UV-Vis spectrometer. A Hitachi S3400N SEM-EDX (SEM-EDX = scanning electron microscope – energy dispersive X-ray) equipment was used to carry out the EDX measurements. Nitrogen adsorption experiments were performed by utilizing a Quantachrome Autosorb iQ-MP volumetric gas adsorption equipment at −196 °C. The degassing of the samples was accomplished at 120 °C under high vacuum for 12 h before the adsorption measurements. The water adsorption measurements were carried out by a volumetric method with a Quantachrome Autosorb iQ MP instrument at 20 °C. Contact angle experiments were performed by employing a KRUSS Drop Shape Analyzer-DSA25 instrument with an automatic liquid dispenser at ambient temperature. A JASCO V-650 UV-Vis spectrophotometer equipped with a 150 mm integrating sphere was used to record the UV-Vis spectra in the solid state. $BaSO_4$ was employed as an internal standard. Fluorescence investigations were performed with a HORIBA JOBIN YVON Fluoromax-4 spectrofluorometer. An Edinburgh Instrument Life-Spec II instrument was employed for measuring the fluorescence lifetimes by using the time-correlated single-photon counting (TCSPC) procedure. The FAST software supplied by Edinburgh

Instruments was utilized to analyse the fluorescence decays by the reconvolution technique.

The synthesis and activation of **2** were performed by following the literature procedure.[37] Regular characterization techniques (N_2 sorption analysis, IR spectroscopy, XRPD as well as TG analysis) were employed for validating the phase-purity.

Synthesis of $[Zr_6O_4(OH)_4(C_8H_2O_4S_2)_6]\cdot DMF\cdot 18H_2O$ (1)

A sealed glass tube containing a mixture of $ZrCl_4$ (50 mg, 0.215 mmol), H_2TDC (49 mg, 0.215 mmol) ligand and benzoic acid (786 mg, 6.45 mmol) in DMF (3 mL) was heated at 150 °C for 24 h by employing a dry block heater. After cooling the tube down to ambient temperature spontaneously, the white precipitate was filtered off and washed several times with acetone. Afterwards, the precipitate was dried in air. Yield: 55 mg (0.02 mmol, 63%) related to the Zr salt. Anal. calcd. for $C_{51}H_{59}NO_{51}S_{12}Zr_6$: C, 25.24 H, 2.45 N, 0.57. Found: C, 24.32 H, 2.88 and N, 0.70%. FT-IR (KBr, cm^{-1}): 3410 (br), 2924 (w), 1507 (m), 1457 (m), 1366 (vs), 1172 (m), 1084 (m), 1021 (m), 884 (m), 771 (m), 721 (s), 658 (m) and 603 (m).

Synthesis of $[Zr_6O_4(OH)_4(C_{15}H_8O_4S_2)_6]\cdot 4DMF\cdot 21H_2O$ (3)

The synthesis procedure for this compound (white powder) was similar to that presented for **1**, except that the H_2MPTDC ligand (68 mg, 0.215 mmol) was used instead of the H_2TDC ligand. Yield: 60 mg (0.018 mmol, 53%) related to the Zr salt. Anal. calcd. for $C_{102}H_{122}N_4O_{57}S_{12}Zr_6$: C, 37.80 H, 3.79 and N, 1.72. Found: C, 38.0 H, 3.68 N, 1.67%. FT-IR (KBr, cm^{-1}): 3422 (br), 3053 (w), 2924 (w), 1573 (m), 1512 (m), 1472(m), 1390 (vs), 1192 (m), 1125 (w), 1027 (m), 775 (m), 720 (m), 666 (s) and 615 (m).

Synthesis of $[Zr_6O_4(OH)_4(C_{20}H_{10}O_4S_2)_6]\cdot 2.5DMF\cdot 11H_2O$ (4)

The synthesis procedure for this compound (white powder) was similar to that presented for **1**, except that the H_2DPTDC ligand (82 mg, 0.215 mmol) was used instead of the H_2TDC ligand and the amount of benzoic acid employed was 262 mg (2.15 mmol) instead of 786 mg (6.45 mmol). Yield: 50 mg (0.015 mmol, 42%) related to the Zr salt. Anal. calcd. for $C_{127.5}H_{91.5}N_{2.5}O_{45.5}S_{12}Zr_6$: C, 46.08 H, 3.14 and N, 1.05. Found: C, 46.8 H, 2.95 N, 1.2%. FT-IR (KBr, cm^{-1}): 3411 (br), 3056(m), 2928 (w), 2858 (w), 1604 (m), 1554 (m), 1515 (s), 1476(m), 1394 (vs), 1222 (m), 1114 (w), 876 (m), 787 (m), 752 (m), 713 (s), 697 (m) and 631 (m).

Activation procedures for the as-synthesized materials

The activation of the as-synthesized forms of all the compounds was carried out in two stages. The stirring of the as-synthesized compounds (0.2 g each) in methanol (30 mL) at room temperature was conducted in the first step. The subsequent step involved collection of the white compounds by filtration and heating them at 100 °C for 24 h under high vacuum. The activated forms of **1**, **2**, **3** and **4** are denoted as **1′**, **2′**, **3′** and **4′**, respectively.

Fluorescence titration experiments

For performing the fluorescence titration experiments, the samples (3 mg each) of **1′**, **2′**, **3′** and **4′** were suspended in water (3 mL) and the mixture was homogenized by ultrasonic treatment for 30 min. Subsequently, 300 μL of each of the suspension was diluted with 2700 μL of water (final concentration = 99 μg mL^{-1}) in a quartz cuvette and 10 mM solutions of different analytes were added in an incremental manner. The calculation of the quenching efficiency (Q) involved the formula: $Q = (1 - I/I_0) \times 100\%$, where I_0 and I are the fluorescence intensity of the aqueous dispersions of the compounds before and after the addition of the analyte. For the Fenton-type reaction, 20 μL of H_2O_2 was added to the aqueous suspension of each compound, accompanied by the addition of Fe^{2+} solution. In the case of the radical scavenging experiment, fluorescence titration measurement was carried out in the presence of 300 μL of isopropyl alcohol (IPA).

Results and discussion

Preparation and activation procedures

Zr(IV)-based MOFs were prepared by using the following ligands: 3,4-dimethylthieno[2,3-*b*]thiophene-2,5-dicarboxylic acid (H_2DMTDC), thieno[2,3-*b*]thiophene-2,5-dicarboxylic acid (H_2TDC), 3,4-diphenylthieno[2,3-*b*]thiophene-2,5-dicarboxylic acid (H_2DPTDC) and 3-methyl-4-phenylthieno[2,3-*b*]thiophene-2,5-dicarboxylic acid (H_2MPTDC). The respective MOF materials were denoted as **1**, **2**, **3** and **4**. The syntheses of all the four MOF compounds involved solvothermal reactions (150 °C, 24 h) in *N*,*N*-dimethylformamide (DMF) using benzoic acid as a modulator. The $ZrCl_4$ to benzoic acid molar ratio was maintained at 1 : 30 for synthesizing **1** and **3**. Compound **4** was prepared by employing a $ZrCl_4$ to benzoic acid molar ratio of 1 : 10. The preparation of **2** was performed by following our formerly reported procedure.[37] The as-synthesized materials contain guest molecules inside their voids, which were first exchanged with methanol. Subsequently, the methanol-exchanged forms of the compounds were subjected to thermal treatment under dynamic vacuum. The thermally activated compounds obtained in this way are termed **1′**, **2′**, **3′** and **4′**.

FT-IR analysis

The activated and as-synthesized forms of **1**, **3** and **4** (Fig. S1–S3, ESI†) display absorption bands with high intensity in the regions of 1560–1600 and 1370–1390 cm^{-1} in their IR spectra. The asymmetric and symmetric stretching vibrations of the coordinated carboxylate groups attached to the ligands give rise to these absorption peaks, respectively.[39–41] The IR spectra of the as-synthesized materials feature absorption peaks at *ca.* 1655 cm^{-1} with moderate intensity. These absorption peaks are observed due to the stretching vibration of the carbonyl groups of the guest DMF molecules.[42] The IR spectra of all the activated compounds lack peaks due to the DMF molecules. These results confirm that the materials have been completely activated.

Structure description

A comparison between the simulated XRPD pattern of the formerly reported, isostructural **2** and the experimental XRPD patterns of the as-synthesized **1**, **3** and **4** reveals that they match quite closely with each other (Fig. 1).[37,43] The indexing of the XRPD patterns of the as-synthesized materials suggests that each of them bears a cubic structure. The resulting lattice parameters are summarized in Table S1, ESI.† The unit cell parameters of **1**, **3** and **4** are similar to those of the recently reported Zr-DMTDC material as well as **2**.[37,43] These similarities indicate that **1**, **3** and **4** possess the UiO-66 (UiO = University of Oslo) framework topology as **2**. The framework structure of Zr(IV),[47] Hf(IV)[48] and Ce(IV)[49]-based pristine UiO-66 materials has been described formerly by several research groups. Similar to the parent UiO-66 compound, the cubic network structure of the presented materials contains $[Zr_6O_4(OH)_4]^{12+}$ building units (Fig. 2). The μ_3-O and μ_3-OH groups occupy the triangular faces of the Zr_6 octahedron. Every Zr atom is coordinated with eight O atoms, forming a square-antiprismatic coordination environment. The O atoms from the carboxylate, μ_3-OH and μ_3-O functionalities occupy the square faces of the square-antiprism. The 3D, cubic framework is constructed by the interconnection of the $[Zr_6O_4(OH)_4]^{12+}$ units with the $-CO_2$ groups of twelve ligands. Larger octahedral as well as smaller tetrahedral cages exist in the framework structures. In the neighbourhood of every octahedral cage, eight tetrahedral cages are present. Narrow triangular windows connect the two types of cages. The inner side of the cages is decorated by the methyl or phenyl groups attached to the coordinated TDC ligands.

It is worth mentioning that compound **4** has less crystallinity (Fig. 1) compared to the other MOFs. It has been documented that the use of bulky ligands for the MOF synthesis usually leads to an amorphous phase of the MOF material.[44,45] The presence of bulky ligands restricts the connectivity between the building blocks and decreases the long-range order. The formation of a large number of basic building units results in 'humps' in the XRPD pattern.[46] In the case of **4**, the presence of two bulky phenyl substituents is responsible for the absence of long-range order in the crystal structure, which results in an amorphous feature in the XRPD pattern.

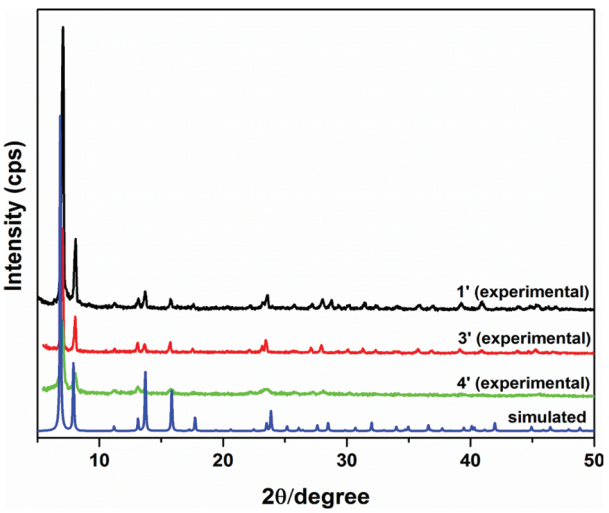

Fig. 1 Simulated and experimental XRPD patterns of **1′**, **3′** and **4′**.

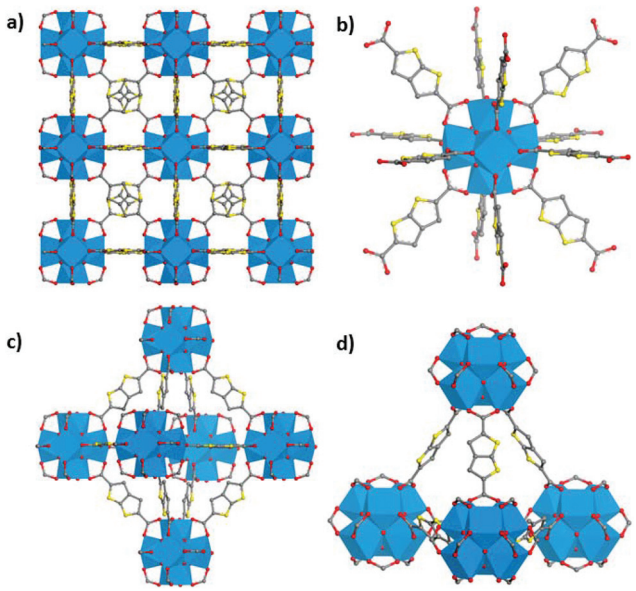

Fig. 2 (a) Cubic 3D framework structure of **1** with a Zr_6 node. (b) Node connectivity for the framework structure of **1**. Views of the (c) octahedral and (d) tetrahedral cages. Colour codes: Zr, blue polyhedra; C, grey; O, red; S, yellow.

Thermal and chemical stability

Thermogravimetric analyses (TG) were performed for examining the thermal stability of the as-synthesized and thermally activated **1**, **3** and **4** (Fig. S4–S6, ESI†). The TG analyses indicate that **1**, **3** and **4** are thermally stable up to 350, 230 and 300 °C, respectively. We have summarized the results of the TG analyses in Table S2, ESI.†

The initial weight loss step (temperature range: 25–130 °C) in the TG traces of the as-synthesized compounds is observed due to the removal of occluded water molecules. In the temperature range of 130–200 °C, the second weight loss step occurs because of the removal of guest DMF molecules. The initial weight loss step (temperature range: 25–130 °C) in the TG traces of activated compounds is noticed owing to the partial hygroscopic characteristics of the materials which results in hydration upon contact with moisture during storage.

To investigate the chemical stability of **1′**, **3′** and **4′**, we stirred the samples in different liquids like acetic acid, water, 1 M HCl and NaOH (pH = 11) under ambient conditions for 6 h. Then, XRPD measurements were accomplished with the filtered materials to check their crystallinity. The XRPD patterns (Fig. S7–S9, ESI†) unambiguously substantiate the retention of the crystallinity of all of the activated compounds after treatment with these liquids. To check the stability of the frame-

work structures of the compounds in the above-mentioned liquids, we have also recorded the UV-Vis spectra of the supernatants. The absorption bands corresponding to the free ligands were observed in the UV-Vis spectra (Fig. S10–S12, ESI†) of all the supernatants. These results suggest the partial framework collapse of the MOF materials. The extent of framework collapse is higher in acetic acid and NaOH solution (pH = 11) compared to that in 1 M HCl and pure aqueous solution.

Gas sorption properties

For proving the permanent porosity, N_2 sorption experiments were conducted with all the activated compounds. From the type-I shaped N_2 adsorption isotherms (Fig. 3), the values of the BET surface areas of the compounds were determined. The estimated BET surface areas of **1′**, **3′** and **4′** correspond to 1299, 978 and 446 $m^2\ g^{-1}$, respectively. The micropore volumes of **1′**, **3′** and **4′**, which were calculated at $p/p_0 = 0.5$, correspond to 0.66, 0.50 and 0.24 $cm^3\ g^{-1}$, respectively. Therefore, the activated materials showed a regular decrease in the values of the surface area and micropore volume with the increase in the bulkiness of the functional groups (methyl and phenyl) attached to the TDC ligand.

Photophysical behaviour

The combination of electronically inert Zr(IV) ions (having the d^{10} configuration) with fluorescent organic ligands has been formerly employed in the literature for the preparation of MOF compounds exhibiting strong luminescence properties.[50,51] Furthermore, the S atoms of the MOF materials incorporating thiophene moieties have been previously shown to act as Lewis basic sites for the recognition of small organic molecules (such as acetone, nitrobenzene and *p*-nitroaniline),[52–54] metal ions (Cu^{2+} and Fe^{3+})[52] and Hg^0 vapour.[43] These observations have inspired us to explore the photoluminescence behaviour of the presented Zr(IV)-based MOF compounds containing thienothiophene-based ligands.

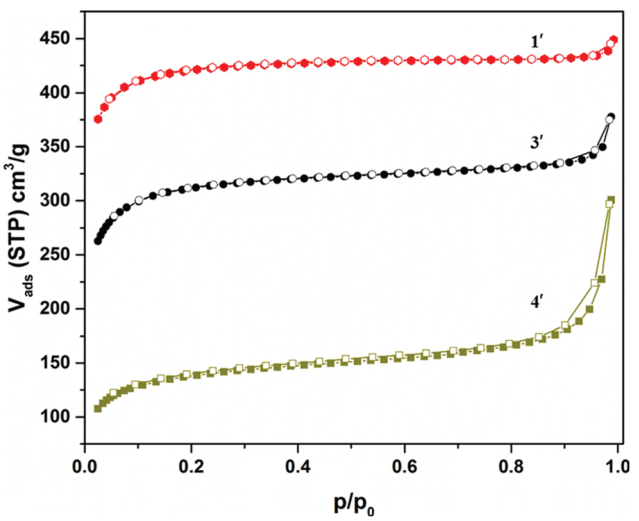

Fig. 3 Nitrogen adsorption (filled symbols) and desorption (empty symbols) isotherms of **1′**, **3′** and **4′** collected at −196 °C.

The diffuse reflectance (DR) UV-Vis spectra of the free ligands as well as the MOF compounds were recorded under ambient conditions. Remarkably, the absorption spectra of the MOF materials are very similar to their corresponding free ligands (Fig. S13–S16, ESI†). The free ligands and the MOF compounds displayed broad absorption bands centred at around 330 nm. These peaks arise owing to the π–π* transition of the ligands.[55–57] These similarities in the absorption spectra point out that the coordinated ligands are solely responsible for the absorption of light in these MOF materials. The optical bandgaps were evaluated for the free ligands and the MOF materials by using the Tauc equation:[58,59]

$$(\alpha h\nu)^2 = A(h\nu - E_g)$$

Here, h stands for the Planck's constant, A is a constant, E_g is the bandgap energy of allowed transitions and ν denotes the frequency of light. The optical bandgaps of **1′**, **2′**, **3′** and **4′** were found to be 3.41, 3.45, 3.44 and 3.43 eV, respectively (Fig. S17–S20, ESI†). These values are comparable to those of the previously reported UiO-66 materials.[60,61] The estimated optical bandgaps of H_2TDC, H_2DMTDC, H_2MPTDC and H_2DPTDC ligands are 3.33, 3.36, 3.28 and 3.34 eV, respectively. Therefore, the optical bandgaps of the free ligands increased upon coordination with the Zr^{4+} ions.

The fluorescence characteristics of the free ligands and the MOF compounds were also studied. The free ligands and the corresponding MOF compounds exhibited broad emission bands centred at around 400 nm in their solid-state fluorescence emission spectra (Fig. S21–S24, ESI†). These emission bands appear because of the π–π* transition of the framework ligands.[62] The similarities in the emission spectra of the free ligands and the corresponding MOF materials suggest that the luminescence of the MOF compounds arises from the ligand-centred π–π* transition. The coordination of the DPTDC ligand with the Zr^{4+} ions is expected to perturb the π–π* transition, causing a blue shift ($\Delta\lambda$ = 7 nm) in the emission band of **4′** compared to the free H_2DPTDC ligand.[51]

The electronic properties of MOFs can be modulated by changing the substituents in the linker molecules.[63] These electronic properties directly influence the other optical properties of MOFs.[64,65] Since all the MOF materials are stable in aqueous medium, their fluorescence properties were explored in pure aqueous medium to check the effect of substitution on their fluorescence behaviour. It can be seen from Fig. 4 that the fluorescence intensity of the compounds (on going from **1′** to **3′**) increases with the increment of electron density in the frameworks. However, the presence of two phenyl groups makes **4′** more hydrophobic compared to other materials. As a result, the aqueous suspension of **4′** shows a slight decrease in the fluorescence intensity compared to that of **3′**. These results suggest that not only the electronic nature of the functional groups but also their hydrophobicity play a crucial role in governing the fluorescence properties of MOF materials.

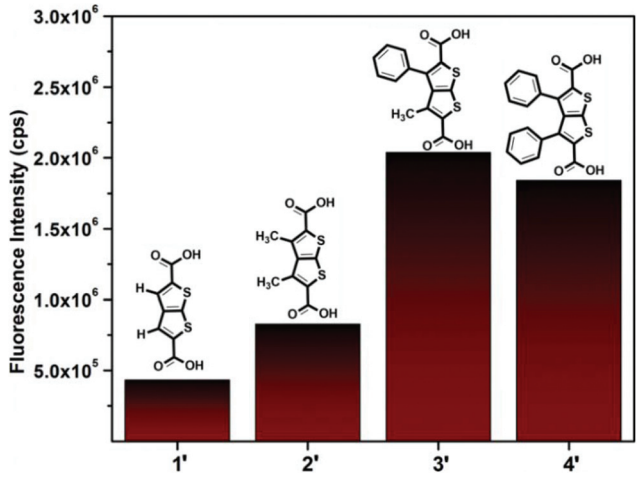

Fig. 4 Ligand-based fluorescence response of the aqueous suspensions of 1′, 2′, 3′ and 4′ under ambient conditions.

Hydrophobic properties

The attachment of water-repellent methyl and phenyl groups to the organic ligands is expected to impart various extents of hydrophobicity in the resulting MOFs. The degree of hydrophobicity of the ligands increases in the order: H_2TDC < H_2DMTDC < H_2MPTDC < H_2DPTDC. For examining the hydrophobicity of the MOF materials, initially water contact angle measurements were performed. With the increase in the degree of hydrophobicity of the ligands, a regular increment in water contact angle (Table 1 and Fig. S25–S28, ESI†) was observed, as expected. The MOF material incorporating the un-functionalized ligand (**1′**) showed the lowest contact angle (~136°). On the other hand, the diphenyl-functionalized material (**4′**) exhibited the highest contact angle (~157°). These results confirm that the attachment of methyl and phenyl groups to the organic ligands introduces different extents of hydrophobicity in the MOF compounds.

The hydrophobic nature of the MOF materials was further confirmed by water sorption experiments. The water uptake capacities of the compounds at p/p_0 = 0.9 are comparable to the maximum water uptake capacities of several well-known MOFs such as MIL-100(Al) (0.5 g g^{-1}), MIL 100(Fe) (0.65–0.75 g g^{-1}),[66,67] Al-fumarate (0.45 g g^{-1}),[68] CAU-10-H (0.33–0.34 g g^{-1}),[69,70] MIL-101(Cr) (1.0–1.5 g g^{-1}),[71,72] pp-MIL-101(Cr) @HIPE (0.29 g g^{-1}; composite with 59 wt% MOF),[73] MIL-100 (Cr) (0.6–0.7 g g^{-1}),[74] and MIL-100(Fe,Cr)@xerogel (0.33 g g^{-1}, composite with 50 wt% MOF; 0.28 g g^{-1}, composite with 51 wt% MOF),[75] and covalent triazine-based frameworks such as Ad2L1 (0.15 g g^{-1}) to Ad4L3 (0.68 g g^{-1}).[76] The water sorption isotherms of the presented MOF compounds (Fig. S22–S25, ESI†) indicate a water uptake above the threshold of 0.3 g g^{-1},[70] however only at higher relative pressures (above a p/p_0 of 0.5). These results indicate that the MOF materials are hydrophobic in nature. The hydrophobicity increases in the order: **1′** < **2′** < **3′** ≪ **4′**. This trend in the hydrophobicity of the MOF compounds is in agreement with that obtained from the water contact angle measurements. Thus, **4′** is the most hydrophobic MOF in the series. Other known MOFs, which are already considered hydrophobic like MIL-101(Cr)[71,75,77–79] or fluorinated MIL-53(Al) and MIL-47,[80] exhibit the major water uptake in the p/p_0 range of 0.4–0.5.[76] In sharp contrast, the existing hydrophilic MOFs such as Al-fumarate and CAU-10-H display the major water uptake with a characteristic S-shaped isotherm, *i.e.*, with a steep increase in the narrow p/p_0 range of ideally between 0.1 and 0.4.[68–70] The XRPD patterns before and after the water sorption experiments do not show any changes, indicating the water stability of the MOFs at least over one water adsorption–desorption cycle (Fig. S29, ESI†).

Table 1 Contact angles and water uptake capacities of the MOF compounds

MOF	Contact angle	Water loading (g g^{-1}) at p/p_0 = 0.5	Water loading (g g^{-1}) at p/p_0 = 0.9
1′	136°	0.30	0.39
2′	148°	0.21	0.35
3′	155°	0.06	0.31
4′	157°	0.04	0.16

Metal ion sensing behaviour

The strong photoluminescence features of the compounds in the solid-state as well as in aqueous medium have encouraged us to investigate their application potential as luminescent probes for the selective, rapid and sensitive sensing of metal ions. In order to serve this purpose, fluorescence titration measurements were performed. 10 mM aqueous solutions of the nitrate salts of various cations (Na^+, K^+, Cd^{2+}, Co^{2+}, Cu^{2+}, Hg^{2+}, Mn^{2+}, Ni^{2+}, Fe^{2+}, Pb^{2+}, Zn^{2+}, Al^{3+}, Cr^{3+} and Fe^{3+}) were gradually added to the well-dispersed aqueous suspensions of all the materials and the fluorescence emission intensities of the compounds were monitored upon excitation at 330 nm at room temperature. Among the 14 metal ions examined, only Fe^{3+} displayed rapid quenching of the fluorescence intensities of all the compounds (Fig. 5 and Fig. S30–S33, ESI†). For the remaining metal ions, the changes in their fluorescence intensities were almost negligible. The highest quenching efficiency was observed for **4′**. The quenching efficiencies of the materials towards Fe^{3+} ions decreased in the order: **4′** (98%) > **3′** (96%) > **2′** (91%) > **1′** (86%). This trend in the quenching efficiency of the compounds can be correlated with the electron density available in their frameworks. Thus, the quenching efficiencies of the materials for Fe^{3+} ions decreased with the decrease in the electron density in the framework compounds.

In order to check the selectivity of all the MOF materials towards Fe^{3+} ions in the presence of other potentially competing metal ions, competitive fluorescence titration experiments were performed. In these competitive titration measurements, fluorescence emission spectra were recorded upon the incremental addition of Fe^{3+} solution to the stable aqueous suspensions of the MOF compounds containing the potentially intru-

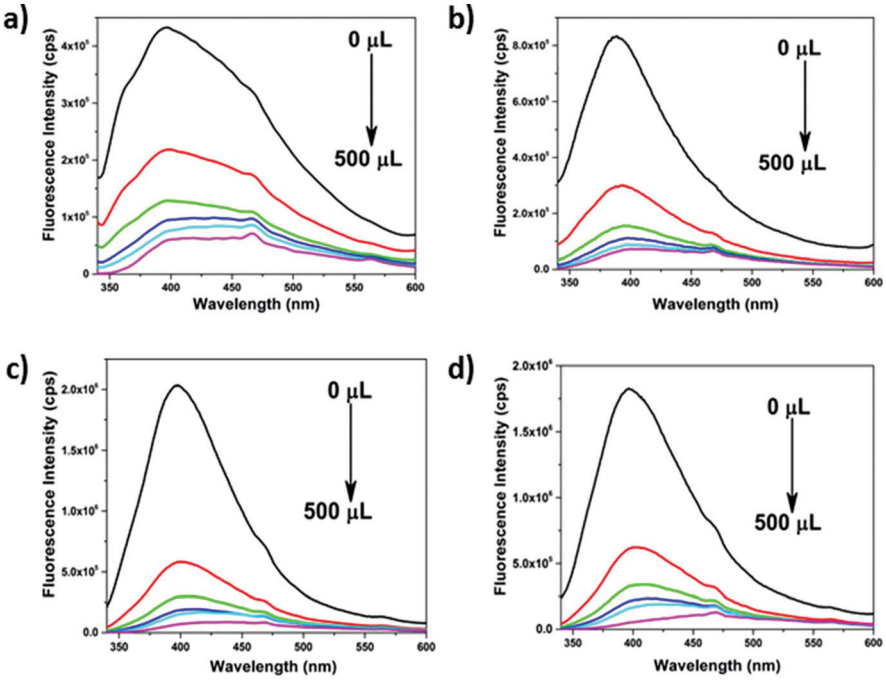

Fig. 5 Quenching of the fluorescence intensity with the gradual addition of Fe^{3+} solution to a 3 mL aqueous suspension of **1′** (a), **2′** (b), **3′** (c) and **4′** (d).

sive metal ions. The changes in the luminescence intensity of **1′**, **2′**, **3′** and **4′** upon the addition of Fe^{3+} solution in the absence and presence of other competing metal ions are presented in Fig. 6 and Fig. S34–37, ESI.† The results of these competitive fluorescence quenching experiments demonstrate that the thienothiophene-based MOF materials are highly selective towards Fe^{3+} ions, even in the presence of other potentially interfering metal ions.

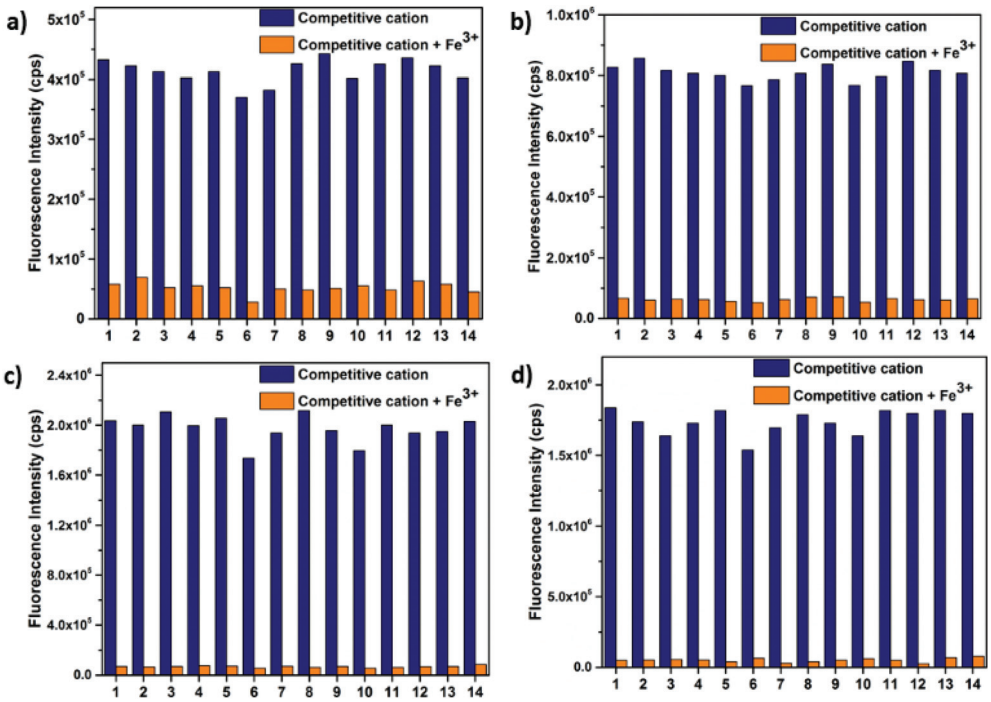

Fig. 6 Change in the fluorescence intensity of **1′** (a), **2′** (b), **3′** (c) and **4′** (d) upon the addition of 500 μL of Fe^{3+} solution in the absence and presence of blank (1), Na^{+} (2), K^{+} (3), Cd^{2+} (4), Co^{2+} (5), Cu^{2+} (6), Hg^{2+} (7), Mn^{2}+ (8), Ni^{2+} (9), Fe^{2+} (10), Pb^{2+} (11), Zn^{2+} (12), Al^{3+} (13) and Cr^{3+} (14) ions.

Stern–Volmer (S–V) quenching constants were calculated by using the following equation:

$$(I_0/I) = K_{sv}[A] + 1$$

where I_0 and I represent the fluorescence intensity of the MOF compound before and after the addition of the analyte, respectively; K_{sv} denotes the quenching constant (expressed in M^{-1}) and [A] symbolizes the molar concentration of the analyte. The analysis of the luminescence quenching data according to the S–V equation allows the quantification of the quenching as well as the determination of the type of the quenching process (static *versus* dynamic). The S–V plots for the quenching of the fluorescence intensities of the MOF materials in the presence of Fe^{3+} ions are shown in Fig. S38–S41 (ESI†). The K_{sv} values for **1′**, **2′**, **3′** and **4′** were estimated to be 4.41×10^3, 8.81×10^3, 10.79×10^3 and 9.10×10^3 M^{-1}, respectively, after excluding the dilution effect. These K_{sv} values compare well with the existing MOF-type fluorescent sensors for Fe^{3+} ions (Table S3, ESI†). The linearity of the S–V plots in a broad concentration range of Fe^{3+} ions suggests that either a dynamic or static quenching process takes place in all the MOF compounds.

For the estimation of the limit of detection (LOD) of the thienothiophene-based MOF materials towards the sensing of Fe^{3+} ions, we gradually added very low concentrations of Fe^{3+} solution to the suspension of the compounds in water and then monitored their fluorescence intensities. By plotting the fluorescence emission intensities of the materials against the concentration of Fe^{3+} solution, linear curves were obtained. From these curves, the LOD values were determined by employing the following equation: LOD = $3\sigma/K$.[81] Here, K stands for the slope of the curves and σ represents the standard deviation of the preliminary fluorescence intensity of MOF materials in the absence of Fe^{3+} solution. The calculated LOD values of **1′**, **2′**, **3′** and **4′** for the sensing of Fe^{3+} ions are 1.26×10^{-6}, 8.57×10^{-7}, 9.33×10^{-7} and 3.4×10^{-7} M, respectively (Fig. S42–S45, ESI†). These LOD values are in agreement with the formerly reported MOF-based fluorescent sensor materials for Fe^{3+} ions (Table S3, ESI†).

The reusability of the fluorescence sensing performances of the MOF probes towards Fe^{3+} ions was examined up to five cycles. For checking their recyclability, the MOF compounds were filtered off after each fluorescence titration experiment. The filtered materials were washed with water repeatedly and then dried in an oven. All the probes showed outstanding recovery of their initial fluorescence intensities, even after five consecutive cycles of fluorescence sensing experiments (Fig. S46–S49, ESI†). As verified by the XRPD experiments (Fig. S50–S53, ESI†), all the MOF materials retained most of their initial crystallinity (thus structural robustness) after five successive cycles of fluorescence titration experiments. Additionally, we checked the effect of pH on the quenching. Fe^{3+} sensing experiments were carried out with solutions having pH values of 2 and 10. The quenching results suggest that a large change in the pH of the sensing medium hardly affects the quenching percentages (Fig. S54, ESI†). These results verify the reusability and high photostability of the MOF probes, which endow them with great potential for the long-term practical sensing of Fe^{3+} ions.

Mechanisms for the detection of Fe^{3+} ions

Three mechanisms have been proposed in the literature for the sensing of Fe^{3+} ions employing MOF materials. They include: (1) collapse of the framework structure,[29] (2) exchange of the framework metal ions by externally added Fe^{3+} ions,[28] and (3) interactions of the Fe^{3+} ions with the coordinated organic ligand.[24] The XRPD patterns (Fig. S50–S53, ESI†) of the MOF materials treated with Fe^{3+} ions were very similar to those of the untreated compounds. The retention of the structural integrity of the MOF compounds after the treatment with Fe^{3+} ions excludes the possibility of the first sensing mechanism. In order to check the possibility of the ion-exchange mechanism, energy-dispersive X-ray (EDX) experiments were accomplished with the MOF materials recovered after the fluorescence sensing experiments. The EDX spectra (Fig. S55–S58, ESI†) reveal that either no Fe^{3+} ions or almost negligible amounts (~0.2 wt%) of Fe^{3+} ions are present in the MOF materials. The insignificant amounts of Fe^{3+} ions might correspond to the Fe^{3+} ions adsorbed in the pores during the fluorescence titration measurements. Therefore, the possibility of the second sensing mechanism can also be ruled out. The third sensing mechanism involving the electronic interactions between the Fe^{3+} ions and framework ligands might be operative in the presented MOF systems. The half-filled 3d ($3d^5$ $4s^0$) orbital of Fe^{3+} ions possesses a high charge density, and thus strong electron-withdrawing character compared to other metal ions.[82] The quenching of the fluorophore moiety by Fe^{3+} ions *via* the electron transfer mechanism has been well-documented for other nanomaterials including MOFs.[83–85] Therefore, we can presume that the electron transfer process from the electron-rich thienothiophene-based ligands to the Fe^{3+} ions might be responsible for the observed fluorescence quenching. The slightly red-shifted fluorescence spectra upon Fe^{3+} addition also support the electron transfer mechansim.[86] For validating the existence of the electron transfer process, the aqueous suspensions of all the MOF materials were treated with the very well-known electron acceptor methyl viologen (MV^{2+}) dications. The fluorescence quenching profiles of the MOF compounds treated with the MV^{2+} dications are very similar to those treated with the Fe^{3+} ions (Fig. S59–S62, ESI†). Since the viologen compounds are very good electron acceptors,[87] the fluorescence quenching can be proposed to occur through the electron transfer process from the electron-rich frameworks to the electron-deficient MV^{2+} dications. The similarity between the florescence quenching profiles obtained with MV^{2+} and Fe^{3+} ions points out that the electron transfer process from the electron-rich frameworks to the electron-deficient Fe^{3+} ions can also be attributed to the luminescence quenching. The fluorescence quenching efficiencies of the MV^{2+} ions follow the order: **1′** (76%) > **2′** (71%) > **3′** (60%) > **4′** (43%). The reverse (*i.e.*, **4′** (98%) > **3′** (96%) > **2′** (91%) > **1′** (86%)) of this trend is found for the quenching with the Fe^{3+}

ions. For MV^{2+} dications (which are relatively larger than Fe^{3+} ions), the increase in steric hindrance and hydrophobicity inside the frameworks owing to the attached functional groups restricts their rates of diffusion through the porous channels, resulting in less interactions with the frameworks, and hence a decrease in the quenching efficiencies. On the other hand, the Fe^{3+} ions are small enough to diffuse rapidly through the porous channels of the MOF compounds, leading to greater interactions with the electron-rich frameworks. As a result, the quenching efficiencies of the Fe^{3+} ions increase with the increasing electron density in the framework materials. Therefore, both steric and electronic factors might be hypothesized to play major roles during the quenching of the fluorescence in these MOF systems.

For realizing the excited-state interactions between the MOF materials and analyte (Fe^{3+} or MV^{2+} ions), time-resolved fluorescence decay experiments were conducted. Upon the gradual addition of Fe^{3+} or MV^{2+} ions, the aqueous suspensions of all the MOF compounds exhibit tri-exponential fluorescence decays with the decrease in the average excited-state lifetime values (Fig. S63–S70 and Tables S4–S7, ESI†). The decrease in the lifetime values of the MOF compounds in the presence of Fe^{3+} or MV^{2+} ions indicates that the fluorescence quenching mechanisms in these systems are dynamic rather than static in nature.

Construction of molecular logic gates

We observed that all the MOFs showed selective sensing properties towards Fe^{3+} ions over other ions including Fe^{2+}, even in the presence of intrusive ions. We further investigated the fluorescence quenching efficiencies of the Fe^{3+} and Fe^{2+}/H_2O_2 systems. The well-known Fenton reaction occurs between Fe^{2+} ions and H_2O_2, which produces Fe^{3+} ions and the hydroxyl radical ($OH^{\bullet}$). The mixture of Fe^{2+} and H_2O_2 showed a rapid quenching of the fluorescence of all the MOF materials (Fig. S71–S74, ESI†). The strongly oxidizing $OH^{\bullet}$ has the ability to capture electrons and can also act as a fluorescence quencher.[88,89] Therefore, $OH^{\bullet}$ can be expected to interfere with the quenching process. To check the effect of $OH^{\bullet}$ on the fluorescence quenching efficiency, we conducted similar fluorescence experiments in the presence of a large excess of isopropyl alcohol (IPA), which is a $OH^{\bullet}$ scavenger.[90] The results of these experiments disclosed that the fluorescence quenching efficiencies are negligibly influenced by the presence of IPA. It can be clearly seen from Fig. S75–S78 (ESI†) that the subsequent addition of the Fe^{2+}/H_2O_2 mixture to the suspensions of MOFs containing IPA triggered rapid fluorescence quenching. Therefore, it can be concluded that the Fe^{3+} ion is solely responsible for the fluorescence quenching. Silva and coworkers demonstrated the first example of a molecular logic gate based on fluorescence signalling.[91] Since their inception in 1993, a large number of molecular logic gates have been described in the literature until now.[92–94] Based on logic operations, the discriminative detection of different analytes has also been reported recently.[95–99] On the other hand, the reports on the construction of MOF-based logic gates are still scarce.[100,101] Based on the selective quenching behaviour of the MOFs towards Fe^{3+} and Fe^{2+}/H_2O_2 systems over Fe^{2+} ions, we have designed a molecular logic gate system (Fig. 7), where Fe^{2+}, Fe^{3+} and H_2O_2 were used as three inputs. The presence and absence of the inputs were defined as '1' and '0', respectively. The quenched and unquenched fluorescence were used as the outputs. The quenched fluorescence was defined as output '1' and the unquenched fluorescence was defined as output '0'. The combination of Fe^{2+} and H_2O_2 was used in the formation of an AND logic gate. On the other hand, Fe^{3+} and the above-described AND logic gate were used in the formation of an OR logic gate. The logic operations were monitored in all eight possible input combinations. It becomes obvious from Fig. S79–S82 (ESI†) that among the eight possible inputs, five inputs [(011), (100), (101), (110) and (111)] showed fluorescence quenching (*i.e.* output 1). The other three inputs [(000), (010) and (001)] exhibited negligible changes in the fluorescence intensity (*i.e.* output 0).

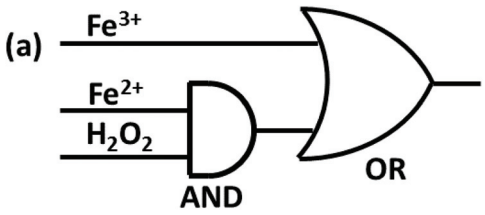

(b)

Input 1 (Fe^{3+})	Input 2 (Fe^{2+})	Input 3 (H_2O_2)	Output (Fluorescence Quenching)
0	0	0	0
1	0	0	1
1	1	0	1
1	0	1	1
0	1	0	0
0	1	1	1
0	0	1	0
1	1	1	1

Fig. 7 (a) Logic gate circuit for AND and OR gates constructed from a three-input system and the corresponding truth table (b).

Conclusions

We have successively synthesized four isoreticular thienothiophene-based Zr(IV) MOF materials under solvothermal conditions. The hydrophobicity and fluorescence properties of all the MOF compounds have been tuned in a systematic fashion by attaching methyl and phenyl groups to the thienothiophene-based ligands. XRPD experiments reveal that the MOF materials retain their structural robustness upon treatment with water, acetic acid, NaOH (pH = 11) and 1 M HCl solutions. Based on the thermogravimetric analyses, the MOF compounds possess moderate to high thermal stability. A combination of contact angle measurements and water sorption ana-

lyses confirms that the attachment of water-repellent methyl and phenyl groups to the ligands imparts different extents of hydrophobicity to the MOF materials. As verified by the fluorescence titration experiments, all the MOF materials featured selective, fast, and sensitive sensing of Fe^{3+} ions in water through the fluorescence quenching mechanism. Thorough experimental studies indicate that the transfer of electrons from the π-conjugated, electron-rich thienothiophene-based frameworks to the half-filled 3d orbitals of Fe^{3+} ions accounts for the fluorescence quenching of MOF compounds. In contrast to the Fe^{3+} ions, the electron acceptor methyl viologen (MV^{2+}) dications displayed a completely reverse trend in the fluorescence quenching efficiencies of the MOF materials. During the elucidation of the reasons for this reverse trend in the quenching efficiency with the MV^{2+} ions, it has been observed that both the steric and electronic effects of the attached functional groups play decisive roles in the luminescence quenching mechanism. In addition, molecular logic gates could be designed by employing the MOFs for distinguishing between Fe^{3+} and Fe^{2+} ions. Overall, high photostability and reusability in Fe^{3+} sensing as well as the ability to discriminate between Fe^{3+} and Fe^{2+} ions through logic operations make the MOFs suitable for real-life applications. We believe that the results of this systematic investigation will provide fruitful insights for understanding the photophysical behaviour of other MOFs and their interactions with different analytes.

Conflicts of interest

The authors declare no conflict of interests.

Acknowledgements

SB acknowledges the Science and Engineering Research Board (SERB; grant no. EEQ/2016/000012), New Delhi for financial support. The analytical facility from Central Instruments Facility (CIF), IIT Guwahati is gratefully acknowledged. CJ thanks the BMBF for grant Optimat 03SF0492C. We are grateful to the Ministry of Human Resource Development for Centre of Excellence in FAST (F. No. 5-7/2014-TS-VII).

Notes and references

1 K. P. Carter, A. M. Young and A. E. Palmer, *Chem. Rev.*, 2014, **114**, 4564–4601.
2 N. Stock and S. Biswas, *Chem. Rev.*, 2012, **112**, 933–969.
3 B. Chen, C. Liang, J. Yang, D. S. Contreras, Y. L. Clancy, E. B. Lobkovsky, O. M. Yaghi and S. Dai, *Angew. Chem.*, 2006, **118**, 1418–1421.
4 O. K. Farha, A. Ö. Yazaydın, I. Eryazici, C. D. Malliakas, B. G. Hauser, M. G. Kanatzidis, S. T. Nguyen, R. Q. Snurr and J. T. Hupp, *Nat. Chem.*, 2010, **2**, 944–948.
5 C. D. Wu, A. Hu, L. Zhang and W. Lin, *J. Am. Chem. Soc.*, 2005, **127**, 8940–8941.
6 T. Ishiwata, Y. Furukawa, K. Sugikawa, K. Kokado and K. Sada, *J. Am. Chem. Soc.*, 2013, **135**, 5427–5432.
7 M.-X. Wu and Y.-W. Yang, *Adv. Mater.*, 2017, **29**, 1606134.
8 L. E. Kreno, K. Leong, O. K. Farha, M. Allendorf, R. P. V. Duyne and J. T. Hupp, *Chem. Rev.*, 2011, **112**, 1105–1125.
9 X. Feng, L. Zeng, D. Zou, Z. Zhang, G. Zhong, S. Peng, L. Liu, L. Chen and J. Zhang, *RSC Adv.*, 2017, **7**, 37194–37199.
10 C. Y. Lee, O. K. Farha, B. J. Hong, A. A. Sarjeant, S. T. Nguyen and J. T. Hupp, *J. Am. Chem. Soc.*, 2011, **133**, 15858–15861.
11 B. Chen, L. Wang, Y. Xiao, F. R. Fronczek, M. Xue, Y. Cui and G. Qian, *Angew. Chem., Int. Ed.*, 2009, **48**, 500–503.
12 K. Müller-Buschbaum, F. Beuerle and C. Feldmann, *Microporous Mesoporous Mater.*, 2015, **216**, 171–199.
13 N. B. Shustova, A. F. Cozzolino, S. Reineke, M. Baldo and M. Dincă, *J. Am. Chem. Soc.*, 2013, **135**, 13326–13329.
14 K. A. Magnus, H. Ton-That and J. E. Carpenter, *Chem. Rev.*, 1994, **94**, 727–735.
15 C. Hsiao, I.-C. Chou, C. D. Okafor, J. C. Bowman, E. B. O'Neill, S. S. Athavale, A. S. Petrov, N. V. Hud, R. M. Wartell and S. C. Harvey, *Nat. Chem.*, 2013, **5**, 525–528.
16 http://www.who.int/water_sanitation_health/dwq/chemicals/iron.pdf.
17 R. R. Crichton, S. Wilmet, R. Legssyer and R. J. Ward, *J. Inorg. Biochem.*, 2002, **91**, 9–18.
18 G. Papanikolaou and K. Pantopoulos, *Toxicol. Appl. Pharmacol.*, 2005, **202**, 199–211.
19 S. J. Dixon and B. R. Stockwell, *Nat. Chem. Biol.*, 2014, **10**, 9–17.
20 L. Zecca, M. B. H. Youdim, P. Riederer, J. R. Connor and R. R. Crichton, *Nat. Rev. Neurosci.*, 2004, **5**, 863–873.
21 B. Wang, Q. Yang, C. Guo, Y. Sun, L.-H. Xie and J.-R. Li, *ACS Appl. Mater. Interfaces*, 2017, **9**, 10286–10295.
22 Y. Dong, H. Zhang, F. Lei, M. Liang, X. Qian, P. Shen, H. Xu, Z. Chen, J. Gao and J. Yao, *J. Solid State Chem.*, 2017, **245**, 160–163.
23 Q. Tang, S. Liu, Y. Liu, J. Miao, S. Li, L. Zhang, Z. Shi and Z. Zheng, *Inorg. Chem.*, 2013, **52**, 2799–2801.
24 X. Y. Dong, R. Wang, J. Z. Wang, S. Q. Zang and T. C. Mak, *J. Mater. Chem. A*, 2015, **3**, 641–647.
25 L. H. Cao, F. Shi, W. M. Zhang, S. Q. Zang and T. C. Mak, *Chem. – Eur. J.*, 2015, **21**, 15705–15712.
26 S. Xing, Q. Bing, L. Song, G. Li, J. Liu, Z. Shi, S. Feng and R. Xu, *Chem. – Eur. J.*, 2016, **22**, 16230–16235.
27 R. Wang, X. Liu, A. Huang, W. Wang, Z. Xiao, L. Zhang, F. Dai and D. Sun, *Inorg. Chem.*, 2016, **55**, 1782–1787.
28 C. X. Yang, H. B. Ren and X. P. Yan, *Anal. Chem.*, 2013, **85**, 7441–7446.
29 S. Dang, E. Ma, Z. M. Sun and H. Zhang, *J. Mater. Chem.*, 2012, **22**, 16920–16926.

30 Y. Zhou, H. H. Chen and B. Yan, *J. Mater. Chem. A*, 2014, **2**, 13691–13697.
31 Z. Xiang, C. Fang, S. Leng and D. Cao, *J. Mater. Chem. A*, 2014, **2**, 7662–7665.
32 D. Feng, Z. Y. Gu, J. R. Li, H. L. Jiang, Z. Wei and H. C. Zhou, *Angew. Chem.*, 2012, **124**, 10453–10456.
33 C. G. Silva, I. Luz, F. X. Llabrs i Xamena, A. Corma and H. García, *Chem. – Eur. J.*, 2010, **16**, 11133–11138.
34 Y. Li, S. P. Singh and P. Sonar, *Adv. Mater.*, 2010, **22**, 4862–4866.
35 I. B. Kim, D. Khim, S. Y. Jang, J. Kim, B. K. Yu, Y. A. Kim and D. Y. Kim, *Org. Electron.*, 2015, **26**, 251–259.
36 N. Kleinhenz, L. Yang, H. Zhou, S. C. Price and W. You, *Macromolecules*, 2011, **44**, 872–877.
37 M. Sk, M. Grzywa, D. Volkmer and S. Biswas, *J. Solid State Chem.*, 2015, **232**, 221–227.
38 W. W. He, G. S. Yang, Y. J. Tang, S. L. Li, S. R. Zhang, Z. M. Su and Y. Q. Lan, *Chem. – Eur. J.*, 2015, **21**, 9784–9789.
39 R. Dalapati and S. Biswas, *Sens. Actuators, B*, 2017, **239**, 759–767.
40 R. Dalapati, B. Sakthivel, A. Dhakshinamoorthy, A. Buragohain, A. Bhunia, C. Janiak and S. Biswas, *CrystEngComm*, 2016, **18**, 7855–7864.
41 A. Das and S. Biswas, *Sens. Actuators, B*, 2017, **250**, 121–131.
42 L. Ge, W. Zhou, V. Rudolph and Z. Zhu, *J. Mater. Chem. A*, 2013, **1**, 6350–6358.
43 K. Wang, H. Huang, W. Xue, D. Liu, X. Zhao, Y. Xiao, Z. Li, Q. Yang, L. Wang and C. Zhong, *CrystEngComm*, 2015, **17**, 3586–3590.
44 T.-H. Chen, A. Schneemann, R. A. Fischer and S. M. Cohen, *Dalton Trans.*, 2016, **45**, 3063–3069.
45 J.-C. Tan, B. Civalleri, C.-C. Lin, L. Valenzano, R. Galvelis, P.-F. Chen, T. D. Bennett, C. M. Draznieks, C. M. Zicovich-Wilson and A. K. Cheetham, *Phys. Rev. Lett.*, 2012, **108**, 095502.
46 T. D. Bennett and A. K. Cheetham, *Acc. Chem. Res.*, 2014, **47**, 1555–1562.
47 J. H. Cavka, S. Jakobsen, U. Olsbye, N. Guillou, C. Lamberti, S. Bordiga and K. P. Lillerud, *J. Am. Chem. Soc.*, 2008, **130**, 13850–13851.
48 M. H. Beyzavi, R. C. Klet, S. Tussupbayev, J. Borycz, N. A. Vermeulen, C. J. Cramer, J. F. Stoddart, J. T. Hupp and O. K. Farha, *J. Am. Chem. Soc.*, 2014, **136**, 15861–15864.
49 M. Lammert, M. T. Wharmby, S. Smolders, B. Bueken, A. Lieb, K. A. Lomachenko, D. D. Vos and N. Stock, *Chem. Commun.*, 2015, **51**, 12578–12581.
50 Y. Bai, Y. Dou, L.-H. Xie, W. Rutledge, J.-R. Li and H.-C. Zhou, *Chem. Soc. Rev.*, 2016, **45**, 2327–2367.
51 M. Sk and S. Biswas, *CrystEngComm*, 2016, **18**, 3104–3113.
52 S. Wang, T. Cao, H. Yan, Y. Li, J. Lu, R. Ma, D. Li, J. Dou and J. Bai, *Inorg. Chem.*, 2016, **55**, 5139–5151.
53 F. Zhang, Y. Wang, T. Chu, Z. Wang, W. Lia and Y. Yang, *Analyst*, 2016, **141**, 4502–4510.
54 Y. Q. Wang, Q. H. Tan, H. T. Liu and Z. L. Liu, *RSC Adv.*, 2015, **5**, 86614–86619.
55 W. Cao, M. Fang, Z. Chai, H. Xu, T. Duan, Z. Li, X. Chen, J. Qin and H. Han, *RSC Adv.*, 2015, **5**, 32967–32975.
56 D. Wang, Q. Guo, H. Gao, Z. Yang, H. Cao, W. He and H. Wang, *RSC Adv.*, 2016, **6**, 59327–59332.
57 M. D. Allendorf, C. A. Bauer, R. K. Bhakta and R. J. T. Houk, *Chem. Soc. Rev.*, 2009, **38**, 1330–1352.
58 M. Usman, S. Mendiratta, S. Batjargal, G. Haider, M. Hayashi, N. R. Gade, J. W. Chen, Y. F. Chen and K. L. Lu, *ACS Appl. Mater. Interfaces*, 2015, **7**, 22767–22774.
59 H. Q. Xu, J. Hu, D. Wang, Z. Li, Q. Zhang, Y. Luo, S. H. Yu and H. L. Jiang, *J. Am. Chem. Soc.*, 2015, **137**, 13440–13443.
60 E. F. Larsen, A. Røyset, J. H. Cavka and K. Thorshaug, *J. Phys. Chem. C*, 2013, **117**, 20610–20616.
61 L. Valenzano, B. Civalleri, S. Chavan, S. Bordiga, M. H. Nilsen, S. Jakobsen, K. P. Lillerud and C. Lamberti, *Chem. Mater.*, 2011, **23**, 1700–1718.
62 L. Zhai, W. W. Zhang, J. L. Zuob and X. M. Ren, *Dalton Trans.*, 2016, **45**, 11935–11938.
63 C.-K. Lin, D. Zhao, W.-Y. Gao, Z. Yang, J. Ye, T. Xu, Q. Ge, S. Ma and D.-J. Liu, *Inorg. Chem.*, 2012, **51**, 9039–9044.
64 T. Musho, J. Li and N. Wu, *Phys. Chem. Chem. Phys.*, 2014, **16**, 23646–23653.
65 T. P. Kaloni, G. Schreckenbach and M. S. Freund, *Sci. Rep.*, 2016, **6**, 36554.
66 F. Jeremias, A. Khutia, S. K. Henninger and C. Janiak, *J. Mater. Chem.*, 2012, **22**, 10148–10151.
67 F. Jeremias, D. Fröhlich, C. Janiak and S. K. Henninger, *New J. Chem.*, 2014, **38**, 1846–1852.
68 F. Jeremias, D. Fröhlich, C. Janiak and S. K. Henninger, *RSC Adv.*, 2014, **4**, 24073–24082.
69 D. Fröhlich, S. K. Henninger and C. Janiak, *Dalton Trans.*, 2014, **43**, 15300–15304.
70 D. Fröhlich, E. Pantatosaki, P. D. Kolokathis, K. Markey, H. Reinsch, M. Baumgartner, M. A. van der Veen, D. E. De Vos, N. Stock and G. K. Papadopoulos, *J. Mater. Chem. A*, 2016, **4**, 11859–11869.
71 J. Ehrenmann, S. K. Henninger and C. Janiak, *Eur. J. Inorg. Chem.*, 2011, **2011**, 471–474.
72 S. K. Henninger, F. Jeremias, H. Kummer and C. Janiak, *Eur. J. Inorg. Chem.*, 2012, **2012**, 2625–2634.
73 M. Wickenheisser and C. Janiak, *Microporous Mesoporous Mater.*, 2015, **204**, 242–250.
74 G. Akiyama, R. Matsuda and S. Kitagawa, *Chem. Lett.*, 2010, **39**, 360–361.
75 M. Wickenheisser, A. Herbst, R. Tannert, B. Milow and C. Janiak, *Microporous Mesoporous Mater.*, 2015, **215**, 143–153.
76 S. Dey, A. Bhunia, I. Boldog and C. Janiak, *Microporous Mesoporous Mater.*, 2016, **241**, 303–315.
77 A. Khutia, H. U. Rammelberg, T. Schmidt, S. Henninger and C. Janiak, *Chem. Mater.*, 2013, **25**, 790–798.
78 M. Wickenheisser, T. Paul and C. Janiak, *Microporous Mesoporous Mater.*, 2016, **220**, 258–269.

79 M. Wickenheisser, F. Jeremias, S. K. Henninger and C. Janiak, *Inorg. Chim. Acta*, 2013, **407**, 145–152.
80 S. Biswas, S. Couck, D. Denysenko, A. Bhunia, M. Grzywa, J. F. Denayer, D. Volkmer, C. Janiak and P. Van Der Voort, *Microporous Mesoporous Mater.*, 2013, **181**, 175–181.
81 A. Buragohain, M. Yousufuddin, M. Sarma and S. Biswas, *Cryst. Growth Des.*, 2016, **16**, 842–851.
82 H. Huang, H. Li, J.-J. Feng, H. Feng, A.-J. Wang and Z. Qian, *Sens. Actuators, B*, 2017, **241**, 292–297.
83 X. Luo, X. Zhang, Y. Duan, X. Wang and J. Zhao, *Dalton Trans.*, 2017, **46**, 6303–6311.
84 M. A. Cardona, C. J. Mallia, U. Baisch and D. C. Magri, *RSC Adv.*, 2016, **6**, 3783–3791.
85 P. Cheng, K.-X. Xu, W. Yao, E. Xie and J. Liu, *J. Lumin.*, 2013, **143**, 583–586.
86 Z. Zhang, F. Li, C. He, H. Ma, Y. Feng, Y. Zhang and M. Zhang, *Sens. Actuators, B*, 2017, **255**, 1878–1883.
87 M. Porel, C. H. Chuang, C. Burda and V. Ramamurthy, *J. Am. Chem. Soc.*, 2012, **134**, 14718–14721.
88 Q. Mei, C. Jiang, G. Guan, K. Zhang, B. Liu, R. Liua and Z. Zhang, *Chem. Commun.*, 2012, **48**, 7468–7470.
89 Y. Song, S. Zhu, S. Xiang, X. Zhao, J. Zhang, H. Zhang, Y. Fu and B. Yang, *Nanoscale*, 2014, **6**, 4676–4682.
90 M. Humayun, Y. Qu, F. Raziq, R. Yan, Z. Li, X. Zhang and L. Jing, *Environ. Sci. Technol.*, 2016, **50**, 13600–13610.
91 P. A. D. Silva, N. H. Q. Gunaratne and C. P. McCoy, *Nature*, 1993, **364**, 42–44.
92 R. Freeman, T. Finder and I. Willner, *Angew. Chem., Int. Ed.*, 2009, **48**, 7818–7821.
93 J. Andreasson and U. Pischel, *Chem. Soc. Rev.*, 2010, **39**, 174–188.
94 W. Lu, Y. Gao, Y. Jiao, S. Shuang, C. Li and C. Dong, *Nanoscale*, 2017, **9**, 11545–11552.
95 A. Rai, A. K. Singh, A. K. Sonkar, A. Prakash, J. K. Roy, R. Nagarajan and L. Mishra, *Dalton Trans.*, 2016, **45**, 8272–8277.
96 N. Sharma, S. I. Reja, V. Bhalla and M. Kumar, *Dalton Trans.*, 2015, **44**, 6062–6068.
97 X. Chai, Y.-X. Fu, T. D. James, J. Zhang, X.-P. He and H. Tian, *Chem. Commun.*, 2017, **53**, 9494–9497.
98 D. Fan, C. Shang, W. Gu, E. Wang and S. Dong, *ACS Appl. Mater. Interfaces*, 2017, **9**, 25870–25877.
99 L. He, J. Li and J. H. Xin, *Biosens. Bioelectron.*, 2015, **70**, 69–73.
100 W. Li, X. Qi, C.-Y. Zhao, X.-F. Xu, A.-N. Tang and D.-M. Kong, *ACS Appl. Mater. Interfaces*, 2017, **9**, 236–243.
101 J. M. Fang, P. F. Gao, X. L. Hu and Y. F. Li, *RSC Adv.*, 2014, **4**, 37349–37352.